Supporting Information

F-coordinated Single-atom Ru Species: Efficient and Durable Catalysts for Photo-Thermal Synergistic Catalytic CO_2 Hydrogenation to Methane

Yunxiang Tang[a], Hao Wang[a], Chan Guo[a], Lige Wang[b], Tingting Zhao[a], Zhengyi Yang[a], Shikang Xiao[a], Jiurong Liu[a], Yanyan Jiang[a], Yufei Zhao[c], Xiao-Dong Wen[d, e], Fenglong Wang[a, *]

[a] Key Laboratory for Liquid-Solid Structural Evolution and Processing of Materials Ministry of Education, Shandong University, Jinan, 250061, P. R. China

[b] Shenzhen Research Institute of Shandong University, Shenzhen, Guangdong, 518057, P. R. China

[c] State Key Laboratory of Chemical Resource Engineering, Beijing University of Chemical Technology, Beijing, 100029, China

[d] State Key Laboratory of Coal Conversion, Institute of Coal Chemistry, Chinese Academy of Sciences, Taiyuan, Shanxi, 030001, P. R. China

[e] National Energy Center for Coal to Liquids, Synfuels China Co., Ltd, Huairou District, Beijing, 101400, P. R. China

***Corresponding Author's Emails:**

fenglong.wang@sdu.edu.cn (F.L.W)

Experimental

Materials

Ruthenium acetate hydrate ($Ru(OAc)_n \cdot xH_2O$), praseodymium nitrate hexahydrate ($Pr(NO_3)_3$ $6H_2O$), aluminium nitrate nonahydrate ($Al(NO_3)_3$ $9H_2O$), ammonium fluoride (NH_4F) and urea were obtained from Shanghai Macklin Biochemical Co., Ltd. All the chemicals were of analytical grade and used as received.

Synthesis of Ru-doping PrAl LDH

Typically, 0.1 mmol of $Ru(OAc)_3$, 1 mmol of $Pr(NO_3)_3$ $6H_2O$, 5 mmol of $Al(NO_3)_3$ $9H_2O$, 2.5 mmol of NH_4F and 10 mmol of urea were dissolved into 30 mL methanol with vigorous stirring for 1 h. The mixture was then transferred into a 100 mL stainless steel autoclave and heated at 150 ℃ for 12 h. Finally, the product was collected by centrifugation and dried at 70 ℃ for 10 h. By changing the molar amount of $Ru(OAc)_3$, Ru-doping PrAl LDH with different Ru contents were prepared.

Synthesis of Ru-F_4 SAs/PA

The Ru-PrF_3/Al_2O_3 (Ru-F_4 SAs/PA) was obtained by calcining the Ru-doping PrAl LDH in 5 vol.% H_2/N_2 stream at 300 ℃ for 2 h with a ramping rate of 3 ℃/min.

Synthesis of Ru-O_4 SAs/PA

The synthesis procedures for Ru-Pr_2O_3/Al_2O_3 (Ru-O_4 SAs/PA) were similar to those of Ru-F_4 SAs/PA, except for the absence of that NH_4F during the preparation of Ru-

doping PrAl LDH.

Synthesis of PrF_3/Al_2O_3 and Pr_2O_3/Al_2O_3

The PrF_3/Al_2O_3 and Pr_2O_3/Al_2O_3 support were also prepared through a similar procedure without introducing the Ru precursor.

Characterizations

A Bruker D8 X-ray diffractometer was employed to record the X-ray diffraction (XRD) patterns with a scanning speed of 4˚/min. The Ru contents were evaluated by an inductively coupled plasma atomic emission spectrometer on an Agilent 7800 instrument. The Brunauer-Emmet-Teller (BET) and Barrett-Joyner-Halenda (BJH) method were employed to measure the specific surface area and pore size distribution on an ASAP2460 instrument. Surface chemical states were analyzed using X-ray photoelectron spectroscopy (XPS, SCIENTIFIC ESCALAB 250Xi). The optical properties of catalysts were evaluated by a Shimadzu UV-3600 spectrophotometer. The aberration-corrected high-angle annular dark-field scanning TEM (HAADF-STEM) images and energy-dispersive X-ray (EDX) elemental mappings were obtained on a TFS Spectra 300 instrument. The X-ray absorption spectra (XAS) at the Ru K-edge of the samples were recorded in the BL 14W1 of Shanghai Synchrotron Radiation Facility (SSRF). A double Si (111) crystal monochromator was used for energy selection. The Athena software package was used to analyze the data. H_2 temperature-programmed reduction (H_2-TPR) measurements were carried out on BELCAT II BelMass instrument. Typically, the sample was initially heated to 300 ℃ with a ramping rate of

10 ℃ min^{-1} in an Ar flow (30 mL min^{-1}) and then cooled to 50 ℃. After that, the sample was heated to 800 ℃ with a ramping rate of 10 ℃ min^{-1} in a 10% H_2/Ar mixed flow (30 mL min^{-1}) atmosphere and the outlet gas was detected by thermal conductivity detector (TCD). CO_2 temperature-programmed desorption (CO_2-TPD) measurements were conducted on BELCAT II BelMass instrument. Typically, the sample was initially heated to 300 ℃ with a ramping rate of 10 ℃ min^{-1} in an He flow (50 mL min^{-1}) and then cooled to 50 ℃. Following this, a 10% CO_2/He mixed flow (50 mL min^{-1}) was introduced to the catalyst bed for 1 h. The sample was then exposed to He (50 mL min^{-1}) for 1 h to remove the physically adsorbed CO_2 from the surface. Finally, the sample was heated to 800 ℃ with a ramping rate of 10 ℃ min^{-1} in a He atmosphere and the outlet gas was detected by TCD.

Photothermal properties measurements

In the photo-to-thermal conversion performance evaluation, the surface temperature change of catalysts with the same distance from light source was measured by the infrared temperature camera (FLIR E8XT). Typically, the samples (50 mg of the catalyst was diluted into 1.2 g of quartz sand) were packed in the same quartz reactor as the one used for catalytic performance evaluation, and then the reactor was irradiated by a 300 W Xe lamp (200-1100 nm, 1.9 W cm^{-2}).

***In situ* diffuse reflectance infrared Fourier transform spectroscopy (*In situ* DRIFTS) analysis**

In situ DRIFTS spectra were collected using a Bruker Vertex 70 spectrometer with a mercury-cadmium-telluride (MCT) detector. The DRIFTS reaction cell (Harrick) was equipped with CaF_2 windows and a heating cartridge. Before the test, the samples were pretreated in 5% vol.% H_2/Ar atmosphere at 300 ℃ for 30 min. Then, the reaction cell was cooled to at room temperature in N_2 to recorded the background spectrum. Subsequently, a mixture of 15 vol.% CO_2, 45 vol.% H_2 and 40 vol.% Ar was introduced into the reaction cell, and the spectra were collected in different temperatures. To simulate the reaction condition of photo-thermal synergistic catalytic CO_2 hydrogenation, an optical fiber equipped with a 300 W Xe lamp was introduced into the reaction cell passing through the quartz window. The spectra were recorded under light irradiation at 250 ℃.

Catalytic performance evaluation

CO_2 hydrogenation experiments were carried out in a continuous flow fixed-bed quartz tubular reactor at atmospheric pressure (Beijing China Education Au-light Co., China, Figure S1). The square-sharped quartz reactor (24 mm × 24 mm) was 2 mm thick, located in the middle of the quartz tube and was placed on a groove carved out to accommodate the tube. In a typical experiment, 50 mg of catalysts powder were diluted with 1.2 g of quartz sands (ca. 0.42 mm in diameter) and then the mixture was packed in the reactor. The set temperature of the reactor was realized by an electronic temperature-controlled furnace. Meanwhile, the actual temperature of catalyst surface under light irradiation was monitored by a thermocouple inserted into the quartz tube

just underneath the catalyst bed. The feed gas consisted of 80 vol % H_2 and 20 vol % CO_2, with a flow rate of 20 mL/min, which corresponds to a GHSV of 24000 mL h^{-1} g_{cat}^{-1}. For the photo-thermal synergistic catalytic CO_2 hydrogenation reaction, a 300 W Xe lamp (λ = 200-1100 nm, 1.9 W cm^{-2}) was used as the light source, which irradiated the catalyst surface through a quartz window and the area for irradiation was 5.76 cm^2. To prevent any gaseous product condensation, the outlet gas line was kept at 120 ℃. The concentrations of CO_2 and products in the effluent gas were periodically analyzed using an online gas chromatograph equipped with a flame ionization detector (FID) and a TCD using N_2 as carrier gas.

The CO_2 conversion (X_{CO2}, %), products selectivity (S, %) and CH_4 production rate (rCH_4) are calculated according to the following equations:

$$X_{CO2}\,(\%) = \frac{n^{CO2,\,in} - n^{CO2,\,out}}{n^{CO2,\,in}} \times 100$$

$$S_{CH4}\,(\%) = \frac{n^{CH4}}{n^{CH4} + n^{CO} + n^{CH3OH}} \times 100$$

$$S_{CH3OH}\,(\%) = \frac{n^{CH3OH}}{n^{CH4} + n^{CO} + n^{CH3OH}} \times 100$$

$$r(CH_4) = \frac{v_{CO2} \times t \times X_{CO2} \times S_{CH4}}{V_m \times m}$$

Where $n_{CO2,\,in}$ and $n_{CO2,\,out}$ are the mole numbers of CO_2 in the inlet and outlet; n_{CH4}, n_{CO} and n_{CH3OH} represent the mole numbers of CH_4 and CH_3OH in the products.

Density functional theory (DFT) calculations

We utilized the Vienna Ab Initio Package (VASP) to conduct density functional theory (DFT) calculations within the generalized gradient approximation (GGA) in the PBE formulation[1]. Projected augmented wave (PAW) potentials were selected to describe the ionic cores and incorporate valence electrons, employing a plane wave basis set with a kinetic energy cutoff of 450 eV.[2-3] Partial occupancies of the Kohn-Sham orbitals were allowed using the Methfessel-Paxton smearing method with a width of 0.05 eV. The electronic energy was considered self-consistent when the energy change was smaller than 10^-5 eV. Geometry optimization was considered convergent when the residual forces were smaller than 0.05 eV/Å. The Gibbs free energy was calculated using the following Equation:

$$\Delta G_{ads} = E_{ads} + \Delta E_{ZPE} - \Delta TS$$

where E_{ads} was the ground energy, ΔE_{ZPE} was the zero-point energy change and ΔS was the entropy change. In this work, the values of ΔE_{ZPE} and ΔS were obtained by vibration frequency calculation.

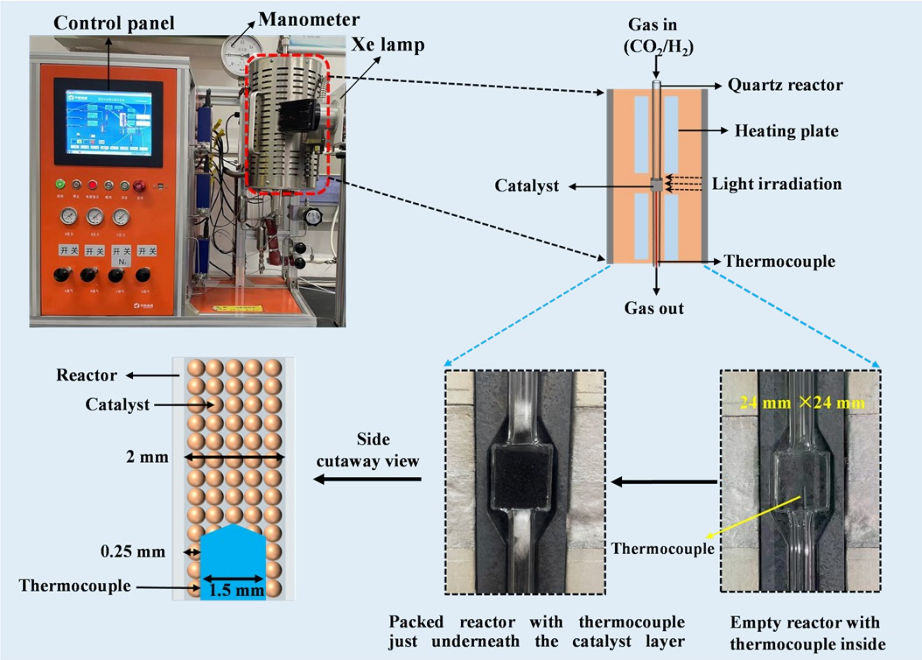

Figure S1. Digital photo of equipment for CO_2 hydrogenation and the schematic illustration of the reactor.

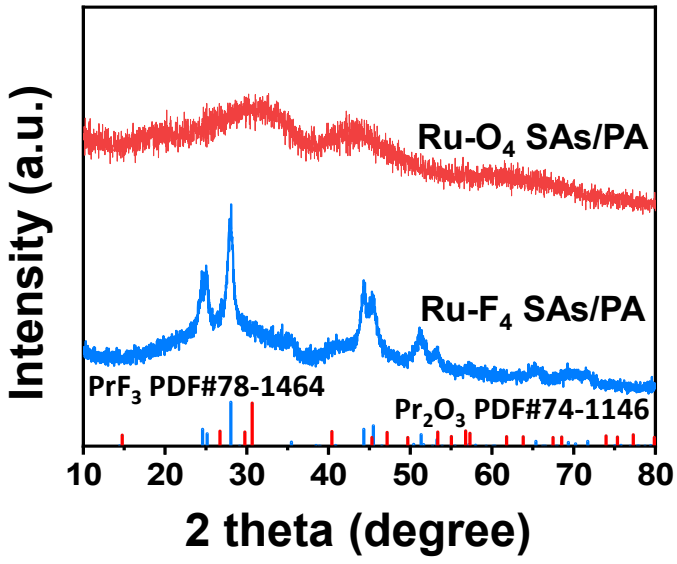

Figure S2. XRD patterns of Ru-F_4 SAs/PA and Ru-O_4 SAs/PA.

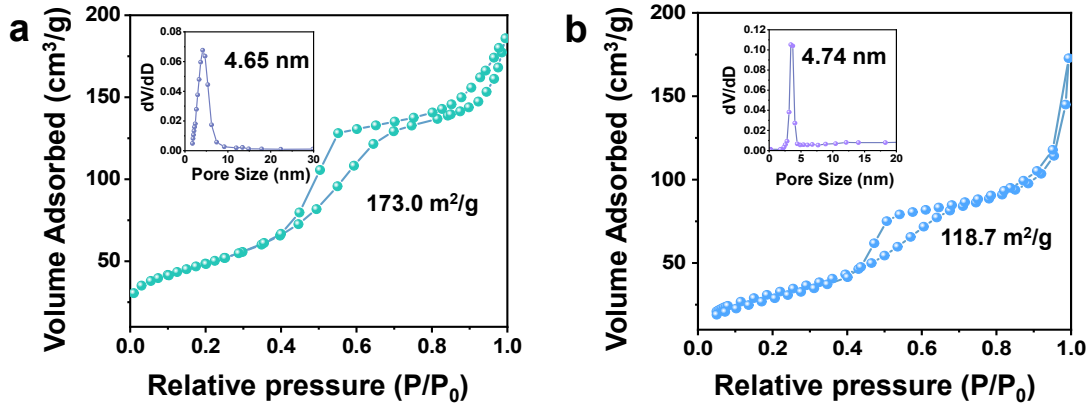

Figure. S3. N_2 adsorption-desorption isotherm of Ru-F_4 SAs/PA and Ru-O_4 SAs/PA. The inset is the corresponding pore size distribution curve.

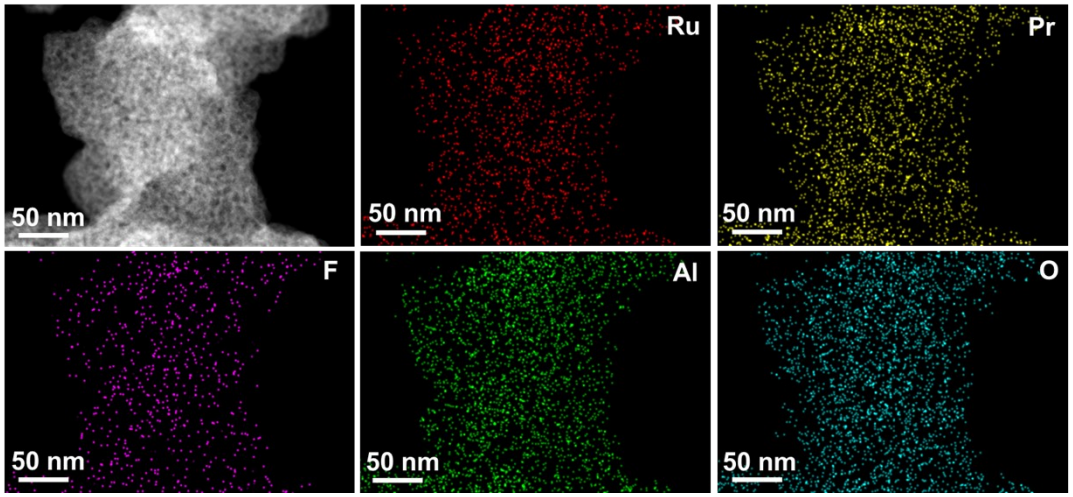

Figure S4. AC-HAADF-STEM images and corresponding EDS mappings of Ru-F_4 SAs/PA.

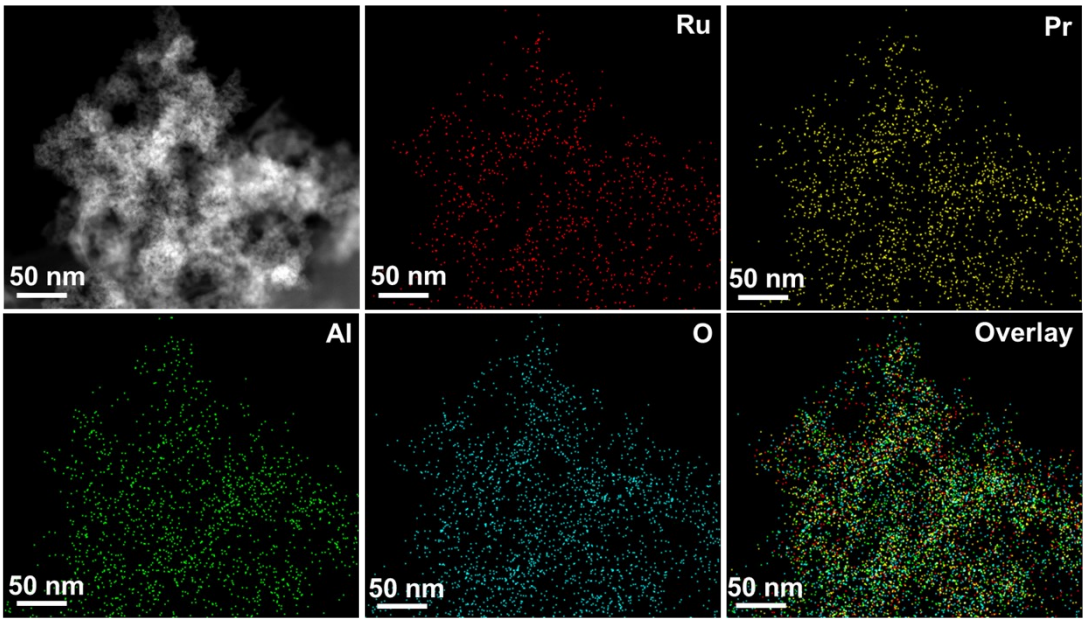

Figure S5. AC-HAADF-STEM images and corresponding EDS mappings of Ru-O_4 SAs/PA.

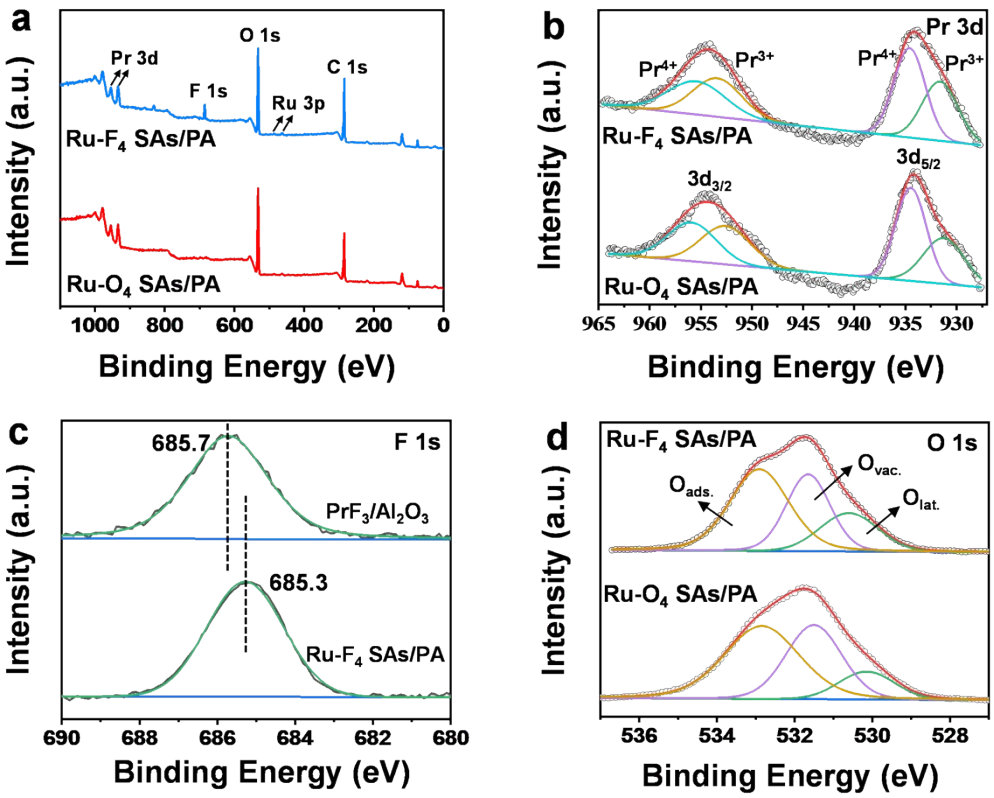

Figure. S6. (a) Survey-scan XPS spectra of Ru-F_4 SAs/PA and Ru-O_4 SAs/PA. High-resolution (b) Pr 3d, (c) F 1s and (d) O 1s XPS spectra of PrF_3/Al_2O_3, Ru-F_4 SAs/PA and Ru-O_4 SAs/PA.

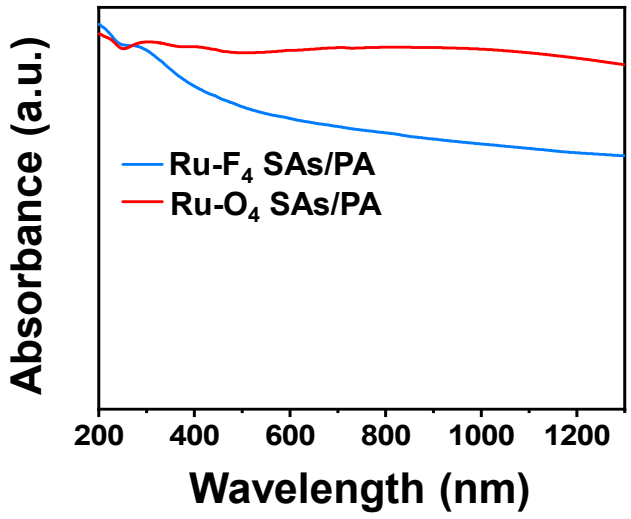

Figure. S7. UV-Vis DRS of Ru-F_4 SAs/PA and Ru-O_4 SAs/PA catalysts.

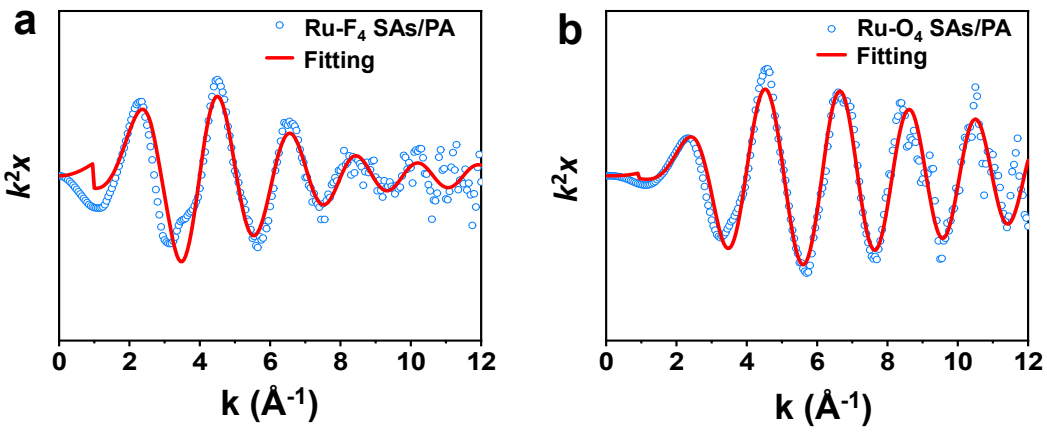

Figure. S8. k space spectra fitting curves for (a) Ru-F_4 SAs/PA and (b) Ru-O_4 SAs/PA.

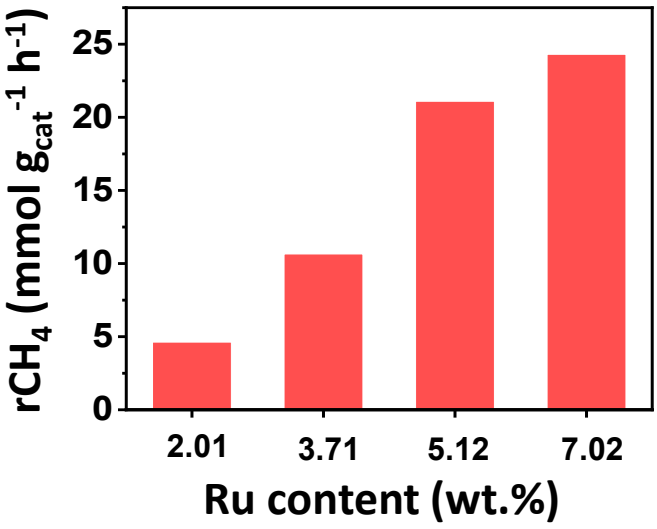

Figure. S9. CH_4 production rate of Ru-F_4 SAs/PA catalysts with different Ru content.

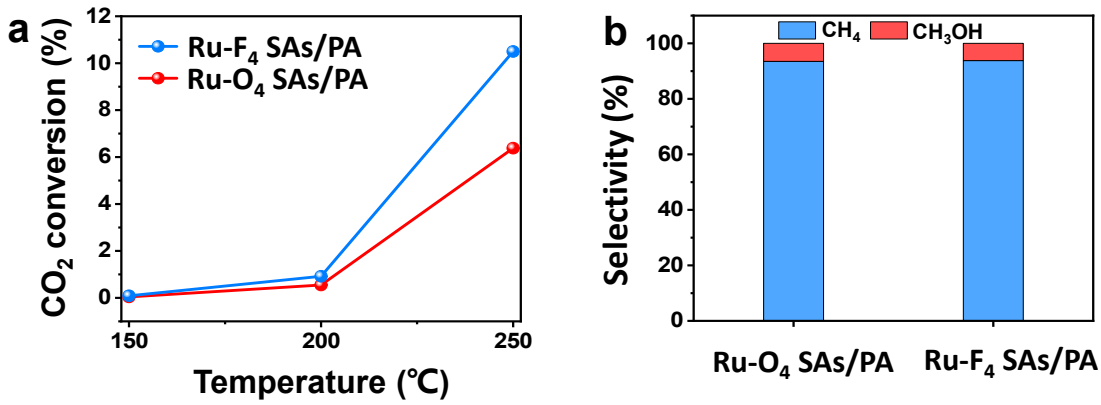

Figure. S10. (a) CO_2 conversion efficiency and (b) product selectivity of Ru-F_4 SAs/PA and Ru-O_4 SAs/PA catalysts.

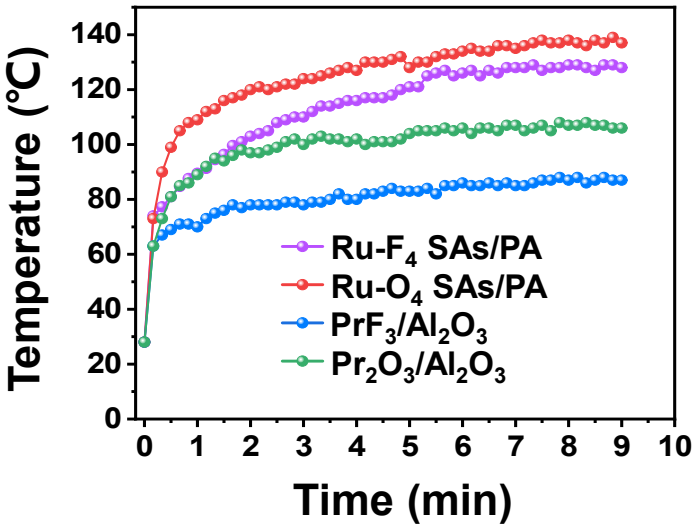

Figure. S11. Surface temperature changes of prepared catalysts under light irradiation (200-1100 nm, 1.9 W cm^{-2}).

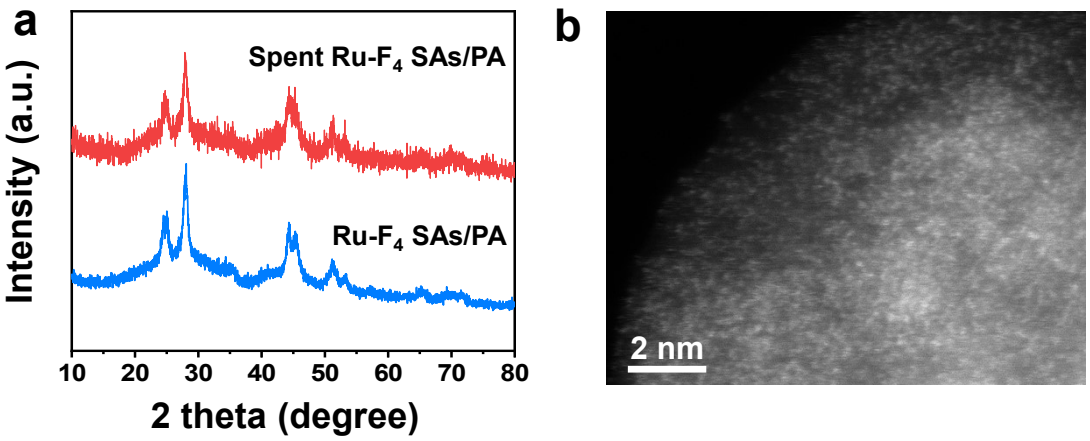

Figure. S12. (a) XRD patterns of Ru-F_4 SAs/PA before and after CO_2 hydrogenation reaction. (b) HAADF-STEM image of spent Ru-F_4 SAs/PA.

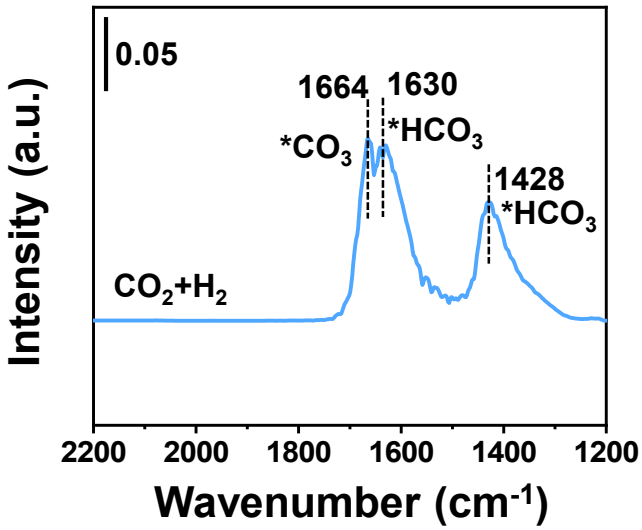

Figure. S13. *In situ* DRIFTS spectra of Ru-F_4 SAs/PA at 30 °C in dark.

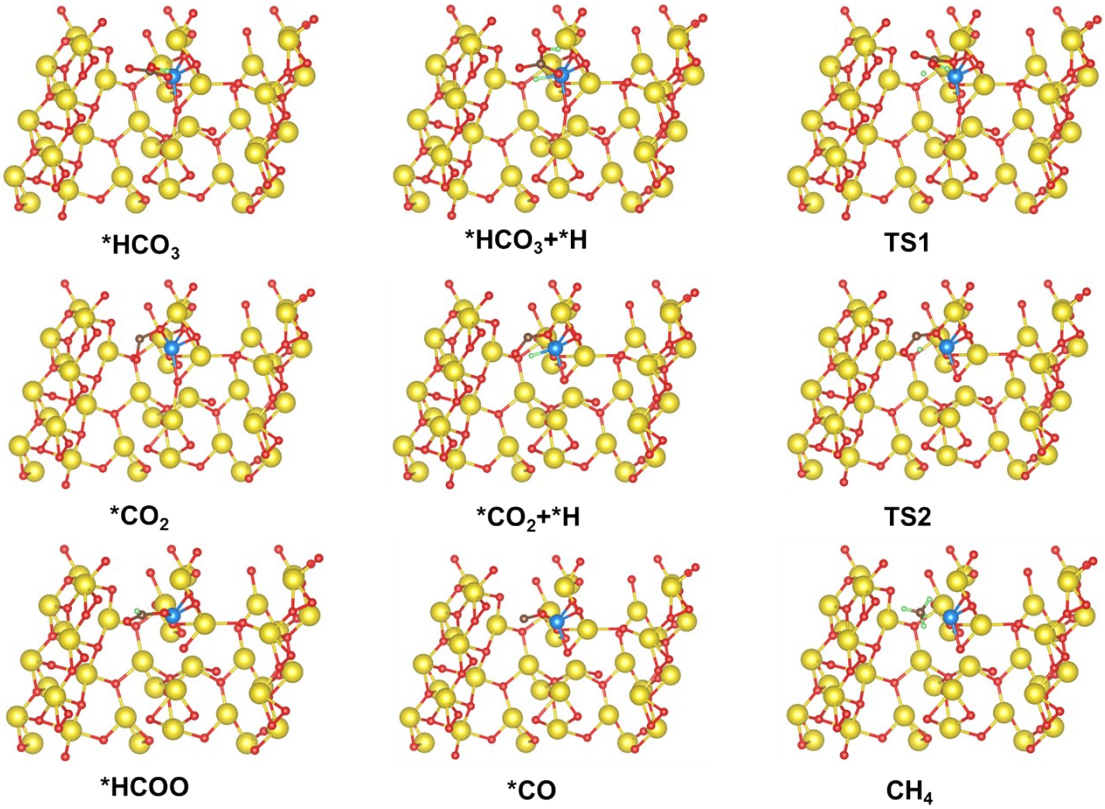

Figure. S14. Optimized geometric structure of the involved intermediates on Ru-O_4 SAs/PA.

Table S1. The loadings for Ru species was confirmed by ICP-OES.

Catalysts	Metal loadings (wt.%)
Ru-F_4 SAs/PA-1	2.01
Ru-F_4 SAs/PA-2	3.71
Ru-F_4 SAs/PA-3	7.02
Ru-F_4 SAs/PA	5.12
Ru-O_4 SAs/PA	5.52

Table S2. Ru K-edge EXAFS fitting results in *R* space for Ru foil and $Ru_{0.88}Co_{0.12}/TiO_2$.

Samples	Paths	C.N.[a]	R (Å)[b]	σ^2(Å^2)[c]	ΔE_0[d]	R factor
Ru foil	Ru-Ru	12	2.67	0.0035	-6.0	0.0080
	Ru-O	6.0	1.98	0.0028	1.1	
RuO_2	Ru-Ru	2.0	3.09	0.0026	-11.5	0.0154
	Ru-Ru	8.0	3.55	0.0029	-3.5	
Ru-F_4 SAs/PA	Ru-F1	1.9	1.93	0.0050	3.6	0.0138
	Ru-F2	2.8	2.07	0.0020		
Ru-O_4 SAs/PA	Ru-O	4.3	2.03	0.0034	3.2	0.0073

[a] coordination numbers; [b] bond distance; [c] Debye-Waller factors; [d] the inner potential correction.

Table S3. The comparison of catalytic activities with other reported catalysts for photo-thermal synergistic catalytic CO_2 methanation.

No. in Graph Figure 3e	Catalyst	Light source	Temperature (°C)	Pressure (MPa)	H_2/CO_2 ratio	CH_4 rate (mmol g_{cat}^{-1} h^{-1})	Selectivity (%)	Ref.
/	Ru-F_4 SAs/PA	300 W Xe lamp 1.9 W/cm^2, Full	200	0.1	4:1	47.4	93.8	This work
1	Pt//$LaCoO_3$	300 W Xe lamp 1.2 W/cm^2, 420-780	200	0.1	4:1	26.07	79	4
2	$Co_7Cu_1Mn_1O_x$	300 W Xe lamp 0.23 W/cm^2, 300-1100	200	0.1	3:1	14.5	85.3	5
3	Ni/BN	300 W Xe lamp Full	230	0.1	4:1	40.57	100	6
4	Ru/TiO_2	300 W Xe lamp 0.1 W/cm^2, 300-1100	250	0.1	3:1	46.15	/	7
5	Ir@UiO-66	300 W Xe lamp 2.3 W/cm^2, Full	250	0.1	4:1	19.9	95	8
6	$Ag_{24}Au$/meso-Co_3O_4	300 W Xe lamp ~0.2 W/cm^2, 350-780	240	1.5	3:1	23	61	9
7	Ni/CeO_2	300 W Xe lamp 420-780	250	/	4:1	0.93	/	10
8	Ru/$MnCo_2O_4$	300 W Xe lamp 1.25 W/cm^2, 420-780	210	0.1	4:1	36.6	96	11
9	Ru/Mg-CeO_2	2.9 W/cm^2, Full	250	0.1	4:1	26	59	12
10	$Ru_{0.10}$@ZrO_2	2.3 W/cm^2, 420-780 LED	300	0.1	4:1	65	100	13
11	Ru/TiO_2	500 W Xe lamp 0.5 W/cm^2, Full	300	/	4:1	72.6	/	14

References

1. G. Kresse and J. Furthmüller, *Phys. Rev. B*, 1996, **54**, 11169.
2. P.E. Blöchl, *Phys. Rev. B*, 1994, **50**, 17953.
3. J.P. Perdew, K. Burke and M. Ernzerhof, *Phys. Rev. Lett.*, 1996, **77**, 3865.
4. L. Wang, Y. Qi, Z. Yang, H. Wu, J. Liu, Y. Tang and F. Wang, *Green Energy and Resources*, 2023, **1**, 100036.
5. Z. He, Z. Li, Z. Wang, K. Wang, Y. Sun, S. Wang, W. Wang, Y. Yang and Z. Liu, *Green Chem.*, 2021, **23**, 5775-5785.
6. X. Zhu, H. Zong, C.J.V. Pérez, H. Miao, W. Sun, Z. Yuan, S. Wang, G. Zeng, H. Xu and Z. Jiang, *Angewandte Chemie*, 2023, **135**, e202218694.
7. C. Wang, S. Fang, S. Xie, Y. Zheng and Y.H. Hu, *J. Mater. Chem. A*, 2020, **8**, 7390-7394.
8. Y. Tang, Z. Yang, C. Guo, H. Han, Y. Jiang, Z. Wang, J. Liu, L. Wu, F. Wang, *J. Mater. Chem. A*, 2022, **10**, 12157.
9. Y. Xiong, X. Liu, Y. Hu, D. Gu, M. Jiang, Z. Tie and Z. Jin, *Nano Res.*, 2022, **15**, 4965-4972.
10. Z. Yang, D. Zheng, X. Yue, K. Wang, Y. Hou, W. Dai and X. Fu, *Appl. Surf. Sci.*, 2023, **615**, 156311.
11. C. Guo, Y. Tang, Z. Yang, T. Zhao, J. Liu, Y. Zhao and F. Wang, *ACS Nano*, 2023, **17**, 23761-23771.
12. Z. Zhang, T. Li, X. Sun, D. Luo, J. Yao, G. Yang, T. Xie, *J. Catal.*, 2024, 430, 115303.
13. F. Almazán, M. Lafuente, A. Echarte, M. Imizcoz, I. Pellejero, L. Gandía, *Chemistry*, 2023, 5, 720-729.
14. H. Zhang, M. Chen, W. Qian, J. Zhang, X. Chen, J. Fang, C. Wang, C. Zhang, *J. Environ. Sci*., 2024, https://doi.org/10.1016/j.jes.2024.05.013.